

# An Optimal Power Allocation Scheme of Microgrid Using Grey Wolf Optimizer

JIANCHENG ZHANG<sup>1</sup>, XINSHENG WANG<sup>1</sup>, AND LINGYU MA<sup>2</sup>

<sup>1</sup>Department of Control Science and Engineering, Harbin Institute of Technology, Weihai 264209, China

<sup>2</sup>Department of Information Engineering, Shandong Management University, Jinan 250000, China

Corresponding author: Xinsheng Wang (wangxsw@126.com)

This work was supported by the Natural Science Foundation of Shandong Province, China, under Grant ZR2017MEE053.

**ABSTRACT** There are some existing power management methods considering economic factors, but these methods are limited by fixed structure of microgrid (MG) and mathematical model, which will be out of effect once the structure changes. In order to obtain the optimal power allocation scheme, this paper proposed the grey wolf optimization (GWO) for the distributed hierarchical control structure of MG, considering the economic dispatching problem. Firstly, the distributed generators (DGs) of MG are considered as multi-agent system, and the secondary controller is constructed. Secondly, the objective function and constraints of GWO are established. Thirdly, the calculation results of GWO are taken as the input of secondary controller, which are called virtual rated power (VRP). Finally, by adjusting VRP dynamically, the on-line real-time optimal power distribution of MG is achieved, and the system stability is proved by multi-agent consensus theory. This power allocation scheme is more flexible to realize the plug-and-play capability. The simulation model is established in Matlab/Simulink environment, and the simulation results show that the method is effective.


**INDEX TERMS** Consensus, grey wolf optimization, microgrid, power allocation, power sharing.

## I. INTRODUCTION

Microgrid (MG) is a distributed system composed of multiple distributed generators (DGs), energy storage and loads. With the intensification of global climate change and the depletion of traditional energy, more and more people are concerned about the use of unconventional and renewable energy for distributed generator (DG), which usually includes wind, solar and nuclear energy etc. [1]. Most of renewable energy generators are distributed and inverter-based. So the control technology of MG becomes particularly important. Due to the different power generation cost of each DG, the total generation cost of MG will vary with the power distribution. Therefore, more attention has been paid to optimizing the use of DG and realizing the optimal economic management of energy resources to reduce cost [2], [3].

There are some existing economic management methods used in MG. An automatic generation control (AGC) proposed in [4], a centralized economic dispatch (ED) program apportions load to generating units to facilitate the governor and AGC functions to run the system in the most economical manner [5]. However, AGC depends on ED signals for

optimal operation and the ED is slower while load keeps changing. An improved method based on AGC and ED is proposed in [6], but it ignores the rated power of each DG and does not achieve power sharing. In [7], economic dispatch was solved by using the method of real population genetic algorithm, which needs actual data as the research basis to optimize the cost of MG. The Grey wolf optimization (GWO) method proposed in [1] and [8], and particle swarm optimization (PSO) algorithm proposed in [9], these two methods used in most literatures need accurate mathematical modeling of each DG. Once disturbance or condition change occurs, the models of each DG will fail. A mixed integer linear programming approach [10] and the technique of conic programming [11] are used to solve the optimal solution of economic dispatch. All the above-mentioned methods are based on fixed structure and mathematical model for economic dispatching. Moreover, they cannot make reasonable economic dispatching in real-time under unexpected conditions and lack the plug-and-play capability as well as flexibility. As the multi-agent consistency algorithm can effectively compensate for these shortcomings, it has been widely used in recent years [12]–[14]. The multi-agent consistency theory is used to realize the active power sharing in [15] and [16]. After changes to the

The associate editor coordinating the review of this manuscript and approving it for publication was Bijoy chand Chand Chatterjee .

topology of MG, the system can adjust the active power dynamically and finally achieve the power-sharing state again. Inspired by this method, if the multi-agent consistency control algorithm is used to realize active and reactive power sharing, then the power of each DG is dynamically managed by adjusting the virtual rated power (VRP as the intermediate variable to regulate the energy, by replacing the rated power of DG in the adjustment process). Eventually dynamic energy management can be achieved.

In order to achieve the lowest cost of energy utilization, the above-mentioned VRP needs to be obtained by multi-objective optimization algorithm. There are many existing optimization methods. Askarzadeh [17] and Bo [18] used genetic algorithm (GA) to minimize the cost of energy production in smart grid. Bahmani-Firouzi and Azizpanah-Abarghoee [19] presented the cost-based formulation to determine the optimal size of the battery energy storage in the operation management of MG based on bat algorithm (BA). A fuzzy self-adaptive PSO algorithm was proposed by Moghaddam *et al.* [20] to optimize a multi-objective operation cost minimization problem of MG considering economy and emission as competitive objectives. In addition, there are GWO proposed by Mirjalili *et al.* [21], firefly optimization algorithm (FOA) proposed by Akbari *et al.* [22] and Moth-flame optimization algorithm (MFO) proposed by Mirjalili [23] etc. Among them, the GWO algorithm is mimicked from the leadership hierarchy and hunting mechanism of grey wolves in nature and is able to provide very competitive results of different benchmark functions compared with other well-known meta-heuristic techniques [21]. Moreover, the exploration and exploitation ability of GWO algorithm is much improved compared with many previously developed optimization techniques [8]. For on-line real-time economic scheduling, the most important point is that outstanding results and superior performance of GWO in terms of solution quality and computational efficiency [24]. Therefore, GWO is applied to solve the operation cost minimization problem of MG here.

In this paper, based on the theory of multi-agent collaborative control and GWO, the optimal control of MG is realized considering economic factors at the secondary control level. Using GWO algorithm, the optimal power allocation scheme of MG is calculated. Subsequently, the VRP of each DG is obtained on basis of these results. Finally, utilizing the nature of consistency, realizes the real-time and dynamic energy management of MG by adjusting VRP. This method not only considers the rated power of each DG, but also takes into account the generation cost of every DG. It improves the flexibility and reliability of the system and realizes the plug-and-play capability. Moreover, this method does not need accurate mathematical modeling for each DG, and a large number of actual data as the research basis. The validity of the method is verified in the MATLAB/SIMULINK environment.

This paper is organized as follows. The structure of the system is shown in Section II. The stability analysis of the

system is in Section III. The simulation results are given in Section IV. Conclusions are made in Section V.

## II. SYSTEM STRUCTURE

Conventional droop control can stabilize the voltage and frequency of MG, the equation (1) is the conventional droop controller's theory [25], where  $\omega^*$  and  $U_{ref}$  are the reference value for the output angular velocity and voltage magnitude respectively,  $P_i$  and  $Q_i$  are the measured active and reactive power at the  $i$ th DG's terminal,  $m_i$  and  $n_i$  are the droop coefficients,  $\omega_n$  and  $U_n$  are nominal frequency and nominal voltage of MG, respectively. With this method however, deviations will produce when the MG switches to islanded mode or a sudden disturbance occurs, and reactive power sharing cannot be achieved. So it is necessary to use secondary control to solve the above problems.

$$\begin{cases} \omega^* = \omega_n - m_i P_i \\ U_{ref} = U_n - n_i Q_i \end{cases} \quad (1)$$

The main circuit structure diagram of MG is shown in Fig.1. The main circuit of AC side adopts LCL filter. Next, the components of the system are introduced in detail.

### A. SECONDARY CONTROL

To obtain reactive power sharing, the secondary control is indispensable to readjust the voltage and frequency of the system. The proposed distributed control framework is shown in Fig.2. Here, the controller based on the consensus algorithm is used as the secondary controller, which includes three control modules: voltage regulator, active power regulator, reactive power regulator.

The voltage and reactive power regulators provide the droop controller with voltage amplitude set-points by generating two corrections  $\delta u_i^1$  and  $\delta u_i^2$ .

The voltage regulator at each node includes an estimator that predicts the average magnitude of the global voltage. The output of the voltage estimator is

$$\bar{u}_i(t) = u_i(t) + \int_0^t \sum_{j \in N_i} a_{ij} (\bar{u}_j(\tau) - \bar{u}_i(\tau)) d\tau \quad (2)$$

where  $a_{ij}$  represents the communication weight when data is exchanged from node  $i$  to  $j$  based on Graph Theory,  $u_i$  is the terminal voltage amplitude of the inverter. Other parameters are shown in Fig. 2.

In the  $i$ th DG, the predicted voltage is compared with the rated voltage  $U_{rate}$  and the deviation is fed back to the PI controller  $G$  to generate the first correction term  $\delta u_i^1$ . The control objective of the voltage regulator is to adjust the average voltage of MG to rated value, but the voltage of each DG may slightly deviate from rated value. So the function of the reactive power regulator is to provide another correction term  $\delta u_i^2$ . This module calculates the deviation from the average

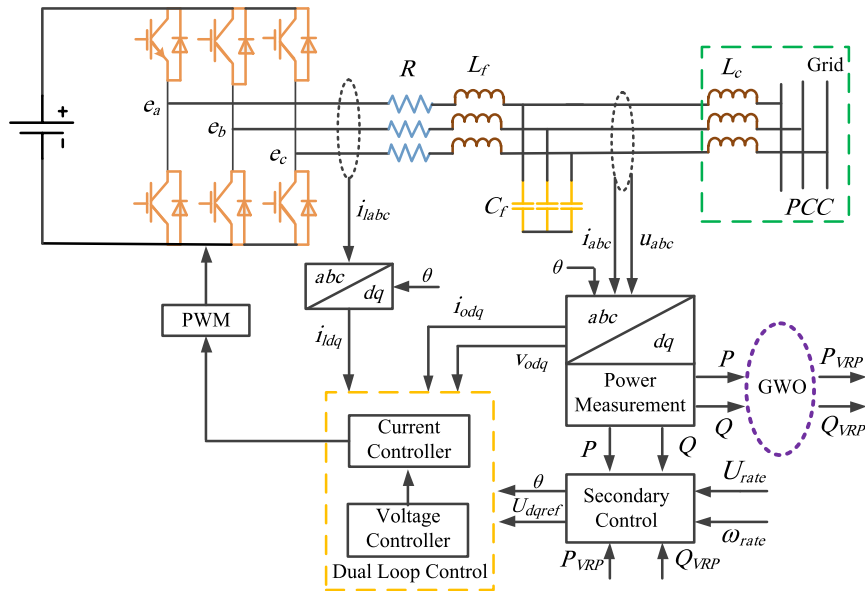


FIGURE 1. Structure block diagram of an inverter-based DG.

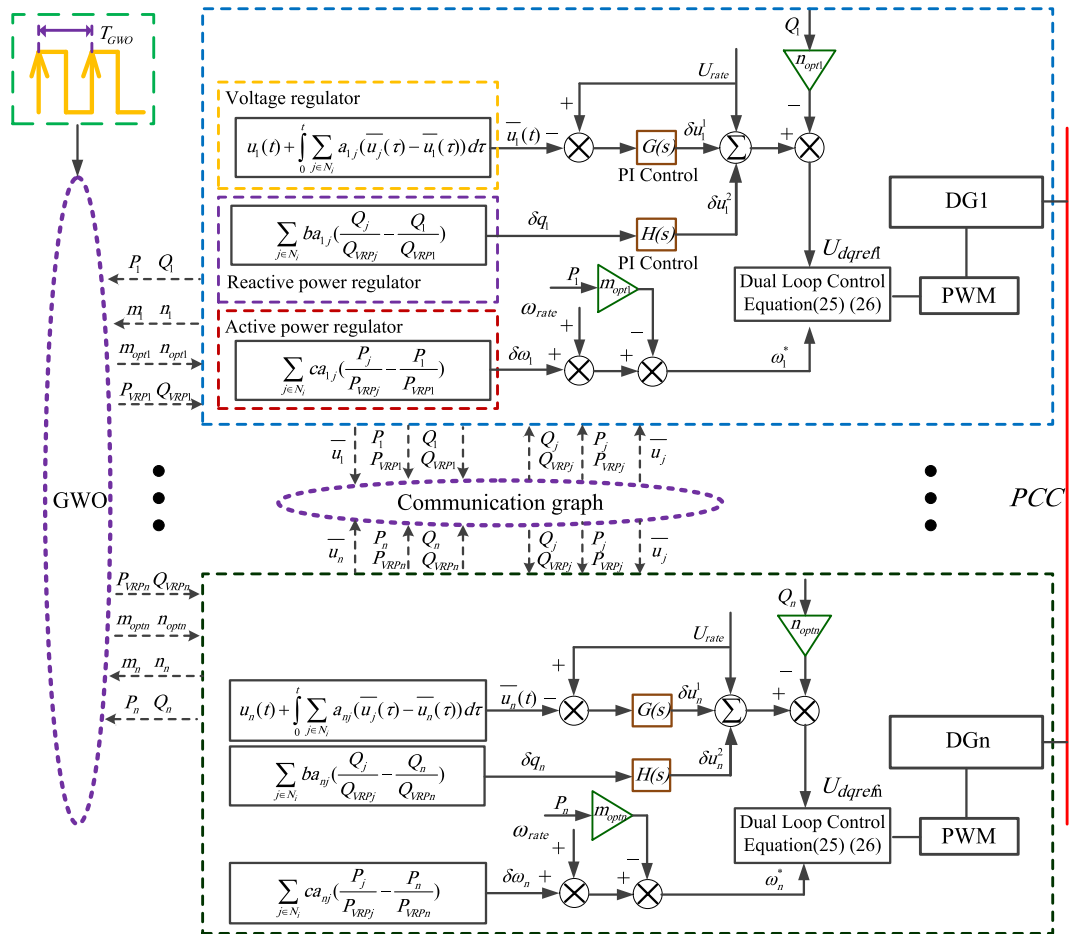


FIGURE 2. Block diagram of the distributed secondary control system.

reactive power of the neighbors.

$$\delta q_i = \sum_{j \in N_i} b a_{ij} \left( \frac{Q_j}{Q_{VRPj}} - \frac{Q_i}{Q_{VRPi}} \right) \quad (3)$$

where  $b$  is a designed parameter. Then the reactive power deviation is fed back into the PI controller  $H$  to adjust the second term of the voltage correction  $\delta u_i^2$ .

The active power regulator at node  $i$  is used to control its frequency and active power. This module calculates the active load mismatch of neighbors and generates the frequency correction term  $\delta\omega_i$

$$\delta\omega_i = \sum_{j \in N_i} ca_{ij} \left( \frac{P_j}{P_{VRPj}} - \frac{P_i}{P_{VRPi}} \right) \quad (4)$$

By the above equations, the system does not require a leader and the phase frequency set-point is

$$\omega_i^*(t) = \omega_{rate} + \delta\omega_i(t) - m_{opti}P_i \quad (5)$$

Set-points of the voltage magnitude on the d-axis and phase angle are as follows:

$$U_{dref} = U_{rate} + \delta u_i^1 + \delta u_i^2 - n_{opti}Q_i \quad (6)$$

$$\theta = \int_0^t \omega_i^*(t) d\tau \quad (7)$$

where the coupling term  $c$  is a designed parameter,  $\delta u_i^1$  and  $\delta u_i^2$  are shown in Fig. 2. In addition, make the set-points of the voltage magnitude on the q-axis  $U_{qref} = 0$  [25].

### B. OVERVIEW OF GREY WOLF OPTIMIZATION

GWO was proposed by Mirjalili et al. [21]. The mathematical model of Grey Wolf algorithm is inspired by the hunting rules of wolves and the social hierarchy of grey wolves. The social hierarchy of grey wolves is divided into four levels, from high to low as alpha ( $\alpha$ ), beta ( $\beta$ ), delta ( $\delta$ ) and omega ( $\omega$ ). Alpha wolves are the highest in the wolf pack. They are the leader of the wolf pack and other wolves must follow their instructions. The second level in the hierarchy of grey wolves is beta. Beta is a subordinate wolf that assists alpha decision-making or other group activities. It reinforces the alpha's commands and gives feedback to the alpha. The lowest ranking grey wolf is omega. They always have to submit to all the other dominant wolves. Delta wolves come in the hierarchy next to the alphas and betas but they lead the omega. To mathematically model the social hierarchy of grey wolves, firstly, the objective function is constructed according to the problems and the best solution is regarded as alpha, the second and third best solutions are considered as beta and delta, while the rests of the solutions are regarded as omega. In addition to the social hierarchy of wolves, the process of group hunting is also an important basis for establishing mathematical models. The steps of grey wolf pack hunting are discussed in the following sections [21].

#### 1) ENCIRCLING PREY

Grey wolves encircle prey during the hunt. In this process, a grey wolf can update its position inside the space around the prey in any random location by using (8) and (9).

$$D = |\xi \cdot S_p(t) - S_w(t)| \quad (8)$$

$$S_w(t+1) = S_p(t) - \sigma \cdot D \quad (9)$$

where  $S_p$  is the position vector of the prey and  $S_w$  indicates the position vector of a grey wolf,  $t$  indicates the current iteration,  $\xi$  and  $\sigma$  are the coefficient vectors which are calculated using the following equations

$$\sigma = 2\mu \cdot r_1 - \mu \quad (10)$$

$$\xi = 2r_2 \quad (11)$$

where components of  $\mu$  are linearly decreased from 2 to 0 over the course of iterations,  $r_1$  and  $r_2$  are random vectors between  $[0, 1]$ .

#### 2) HUNTING

The hunt is guided by the alpha wolf. The beta and delta wolves participate in hunting occasionally. To mathematically represent the hunting behavior of grey wolves, it is supposed that the alpha, beta and delta wolves have better knowledge about the potential location of prey. Therefore, the first three best solutions achieved are saved and the other search agents are forced to update their positions according to the position of the best search agents. The following equations can be used in this regard [21].

$$D_\alpha = |\xi_1 \cdot S_\alpha - S_w|, \quad D_\beta = |\xi_2 \cdot S_\beta - S_w|, \quad D_\delta = |\xi_3 \cdot S_\delta - S_w| \quad (12)$$

$$S_{w1} = S_\alpha - \sigma_1 \cdot D_\alpha, \quad S_{w2} = S_\beta - \sigma_2 \cdot D_\beta, \quad S_{w3} = S_\delta - \sigma_3 \cdot D_\delta \quad (13)$$

$$S_w(t+1) = \frac{S_{w1} + S_{w2} + S_{w3}}{3} \quad (14)$$

#### 3) ATTACKING PREY (EXPLOITATION)

The grey wolves finish their hunting process by attacking the prey when it stops moving. In order to establish the mathematical model of grey wolf approaching prey, the value of  $\mu$  is gradually reduced from 2 to 0 over the course of iterations and thereby the fluctuation range of  $\sigma$  is also decreased. When random values of  $\sigma$  are in  $[-1, 1]$ , then the next position of a search agent can be in any position between its current position and the position of the prey, when  $|\sigma| < 1$ , the grey wolves attack the prey.

#### 4) SEARCH FOR PREY (EXPLORATION)

In order to avoid the local optimal solution to search for a fitter prey, grey wolves diverge from each other. In order to mathematically model the divergence characteristics of grey wolves,  $\sigma$  is employed with random values greater than 1 or less than  $-1$  to oblige the search agent to diverge from the prey. This puts emphasis on exploration characteristics and allows the GWO algorithm to search globally, when  $|\sigma| > 1$ , the grey wolves diverge from the prey to find a fitter prey.

#### 5) CONSTRAINTS

Considering the economic factors of energy management, the desired target is regarded as prey, and the optimal position of wolves is the optimal solution to the problem. In this paper,

the construction of objective function is shown in (15).

$$f = \eta f_1 + \lambda f_2 \quad (15)$$

$$f_1 = A_1(P_{Mag1} + Q_{Mag1}) + A_2(P_{Mag2} + Q_{Mag2}) + \dots + A_n(P_{Magn} + Q_{Magn}) \quad (16)$$

$$f_2 = \sum_{i=1}^n (\sqrt{(P_{ratei} - P_{Magi})^2 + P_{Magi}^2} + \sqrt{(Q_{ratei} - Q_{Magi})^2 + Q_{Magi}^2}) \quad (17)$$

where  $\eta$  and  $\lambda$  are weight coefficients, the  $f_1$  function is the cost of generating electricity throughout the system.  $P_{Magn}$  and  $Q_{Magn}$  are the active and reactive power, respectively, which should be emitted by  $n$ th DG after calculation based on GWO.  $A_i$  is the cost coefficient of the  $i$ th DG. The  $f_2$  function is to consider the actual rated power of each DG to avoid the DG with large rated power generating less power and full load operation.

According to [10], the  $A_i$  in (16) is a comprehensive cost coefficient. In order to facilitate the calculation and verify the effectiveness of the method, it is simplified and scaled, as shown in Table I.

Based on the law of conservation of energy, the optimized power should be equal to the power before optimization, there are

$$\sum_{i=1}^n P_i = \sum_{i=1}^n P_{Magi}, \quad \sum_{i=1}^n Q_i = \sum_{i=1}^n Q_{Magi} \quad (18)$$

In addition, the optimized power  $P_{Magi}$  and  $Q_{Magi}$  should be less than the actual rated power  $P_{ratei}$  and  $Q_{ratei}$ , respectively. As shown in (19).

$$\begin{aligned} 0 &\leq P_{Magi} \leq P_{ratei}, \\ 0 &\leq Q_{Magi} \leq Q_{ratei}, \quad i = 1, 2, \dots, n \end{aligned} \quad (19)$$

To achieve active and reactive power sharing, the following conditions should also be satisfied.

$$m_{opt1}P_{Mag1} = m_{opt2}P_{Mag2} = \dots = m_{optn}P_{Magn} \quad (20)$$

$$n_{opt1}Q_{Mag1} = n_{opt2}Q_{Mag2} = \dots = n_{optn}Q_{Magn} \quad (21)$$

where  $m_{opti}$  and  $n_{opti}$  are the active and reactive droop coefficients of  $i$ th DG after calculation based on GWO, respectively. Finally, the virtual rated power of DG is derived from the actual rated power and the optimized power, as shown in (22)-(24). The process of proof is described in section III.

$$\varepsilon_P = \min \left( \frac{P_{rate1}}{P_{Mag1}}, \frac{P_{rate2}}{P_{Mag2}}, \dots, \frac{P_{raten}}{P_{Magn}} \right) \quad (22)$$

$$\varepsilon_Q = \min \left( \frac{Q_{rate1}}{Q_{Mag1}}, \frac{Q_{rate2}}{Q_{Mag2}}, \dots, \frac{Q_{raten}}{Q_{Magn}} \right) \quad (23)$$

$$P_{VRPi} = \varepsilon_P \times P_{Magi}, \quad Q_{VRPi} = \varepsilon_Q \times Q_{Magi}, \quad i = 1, 2, \dots, n \quad (24)$$

The flow-chart of power management of MG is depicted based on GWO algorithm, as shown in Fig.3. In addition, in order to speed up the simulation, the GWO module is

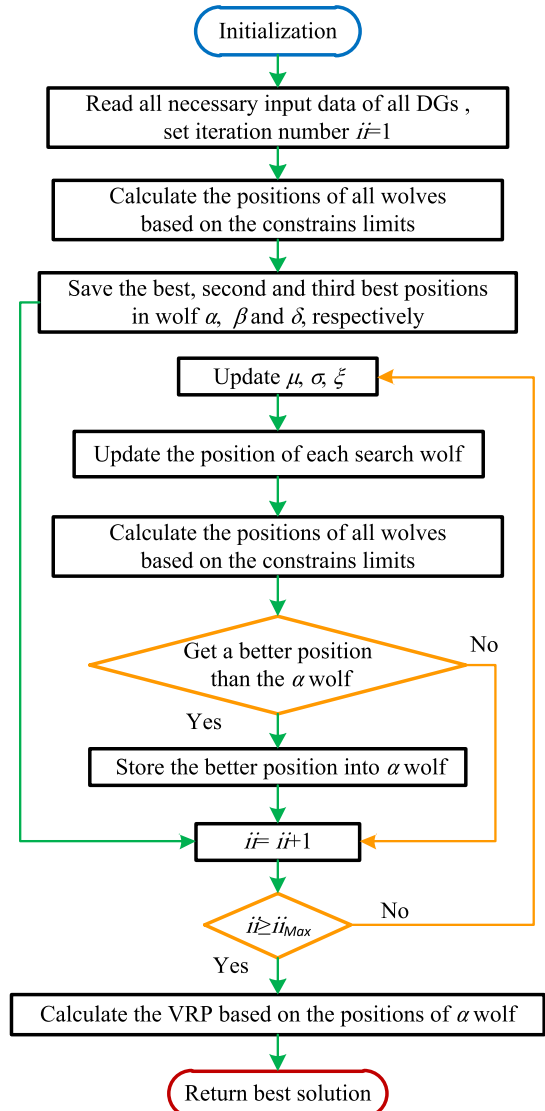


FIGURE 3. Flowchart of the grey wolf optimizer algorithm.

triggered every time  $T_{GWO}$ , as shown in Fig.2. The value of  $T_{GWO}$  is adjusted according to the actual needs, and GWO is triggered when  $t = 7.5s$  in this paper.

### C. DUAL LOOP CONTROL

The secondary controller outputs the reference voltage. After that the PWM control signal is generated through the voltage and current control loop of DG to control the AC inverter. The design of dual loop control is referred to in [25]. The voltage controller and current controller are usually combined with droop control in circuit, which can stabilize voltage and frequency and realize plug-and-play. The model of the voltage loop is shown in (25), where  $K_{PV}$  and  $K_{IV}$  are the gain and integral coefficients of the voltage loop PI controller, respectively.  $C_f$  is the capacitance of the filter.  $i_{ld}^*$  and  $i_{lq}^*$  are the reference current d and q axis components of the current loop, respectively. The model of the current loop

is shown in (26):

$$\begin{cases} i_{ld}^* = Fi_{od} - \omega_{ref} C_f v_{oq} + K_{PV}(U_{dref} - v_{od}) \\ \quad + K_{IV} \int (U_{dref} - v_{od}) dt \\ i_{lq}^* = Fi_{oq} + \omega_{ref} C_f v_{od} + K_{PV}(U_{qref} - v_{oq}) \\ \quad + K_{IV} \int (U_{qref} - v_{oq}) dt \end{cases} \quad (25)$$

$$\begin{cases} v_{PWMd} = -\omega_{ref} L_f i_{lq} + K_{PI}(i_{ld}^* - i_{ld}) \\ \quad + K_{II} \int (i_{ld}^* - i_{ld}) dt \\ v_{PWMq} = \omega_{ref} L_f i_{ld} + K_{PI}(i_{lq}^* - i_{lq}) \\ \quad + K_{II} \int (i_{lq}^* - i_{lq}) dt \end{cases} \quad (26)$$

where  $K_{PI}$  and  $K_{II}$  are the gain and integral coefficients of the current loop PI controller, respectively.  $L_f$  is the inductor of the filter.  $\omega_{ref}$  is the nominal angular frequency.  $v_{PWMd}$  and  $v_{PWMq}$  are the reference voltage d and q axis components of the PWM, respectively.

### III. STEADY-STATE ANALYSIS

In this section, the stability of the system is analysed, which proves that the proposed method can achieve the active and reactive power sharing, meanwhile, the dynamic management of energy is obtained. Based on the control structure in Fig. 2, the correction terms  $\delta u_i^1$  and  $\delta u_i^2$  are

$$\delta u_i^1 = G(U_{rate} - \bar{u}_i) \quad (27)$$

$$\delta u_i^2 = H \cdot \delta q_i \quad (28)$$

for the whole system, the above equations can be written as

$$\delta \mathbf{u}^1 = \delta \mathbf{u}_0^1 + (\mathbf{G}_P + \mathbf{G}_I(t - t_0))(U_{rated} - \bar{\mathbf{u}}) \quad (29)$$

$$\delta \mathbf{u}^2 = \delta \mathbf{u}_0^2 + (\mathbf{H}_P + \mathbf{H}_I(t - t_0))\delta \mathbf{q} \quad (30)$$

where  $\mathbf{G}_I$  and  $\mathbf{G}_P$  are the diagonal matrices carrying the integral and proportional gains of the voltage-controller matrix  $\mathbf{G}$  such that  $\mathbf{G}_P + \mathbf{G}_I/s = \mathbf{G}$ . Similarly,  $\mathbf{H}_I$  and  $\mathbf{H}_P$  are the diagonal matrices carrying the integral and proportional gains of the  $Q$ -controller matrix  $\mathbf{H}$ .  $\bar{\mathbf{u}} = [\bar{u}_1, \bar{u}_2, \dots, \bar{u}_n]^T$  denotes the voltage estimation vector,  $\delta \mathbf{u}_0^1$  and  $\delta \mathbf{u}_0^2$  are column vectors that carry the integrator outputs in  $\mathbf{G}_I$  and  $\mathbf{H}_I$  at  $t = t_0$ , respectively.  $U_{rate} \in \mathbf{R}^{N \times 1}$  whose elements are all  $U_{rate}$ .

Take the differential of the output of voltage estimator (2)

$$\begin{aligned} \dot{\bar{u}}_i(t) &= \dot{u}_i(t) + \sum_{j \in N_i} a_{ij}(\bar{u}_j(t) - \bar{u}_i(t)) \\ &= \dot{u}_i(t) + \sum_{j \in N_i} a_{ij}\bar{u}_j(t) - d_i^{in}\bar{u}_i \end{aligned} \quad (31)$$

Accordingly, the global observer dynamic is

$$\begin{aligned} \dot{\bar{\mathbf{U}}} &= \dot{\mathbf{U}} + \mathbf{A}_G \bar{\mathbf{U}} - \mathbf{D}_G^{in} \bar{\mathbf{U}} \\ &= \dot{\mathbf{U}} + (\mathbf{A}_G - \mathbf{D}_G^{in}) \bar{\mathbf{U}} \\ &= \dot{\mathbf{U}} - \mathbf{L} \bar{\mathbf{U}} \end{aligned} \quad (32)$$

Therefore, the above equation is expressed in frequency domain as

$$\bar{\mathbf{U}} = s(\mathbf{I}_N + \mathbf{L})^{-1} \mathbf{U} \quad (33)$$

where  $\mathbf{I}_N \in \mathbf{R}^{N \times N}$ ,  $\mathbf{u} = [u_1, u_2, \dots, u_n]^T$  is the voltage measurement vector, which carries measured voltage of all

nodes.  $\mathbf{U}$  and  $\bar{\mathbf{U}}$  are the Laplace transforms of  $\mathbf{u}$  and  $\bar{\mathbf{u}}$ , respectively.  $\mathbf{A}_G$  represents the communication weight matrix based on Graph Theory,  $\mathbf{D}_G^{in} = \text{diag} \{d_i^{in}\}$  is a diagonal matrix with  $d_i^{in} = \sum_{j \in N_i} a_{ij}$ ,  $\mathbf{L}$  is Laplacian matrix.

*Lemma 1* [26], [27]: If the communication graph has a spanning tree with a balanced Laplacian matrix,  $\mathbf{L}$ , then, the matrix  $\mathbf{L}$  has a single eigenvalue at the origin, i.e.,  $\lambda_1 = 0$  and other eigenvalues lie in the open left hand plane (OLHP). Meanwhile, the following equation holds

$$\lim_{s \rightarrow 0} s(\mathbf{I}_N + \mathbf{L})^{-1} = \mathbf{M} \quad (34)$$

where  $\mathbf{M} \in \mathbf{R}^{N \times N}$  is the averaging matrix, whose elements are all  $1/N$ .

*Theorem 1:* If the associated Laplacian matrix  $\mathbf{L}$  is balanced, then, using the observer in (33), all elements of  $\bar{\mathbf{u}}$  converge to a consensus value, which is the true average voltage, i.e., the average of all elements in  $\mathbf{u}$ . Equivalently,

$$\bar{\mathbf{u}}_{sat} = \mathbf{M} \mathbf{u}_{sat} = \langle \mathbf{u}_{sat} \rangle \mathbf{I} \quad (35)$$

where  $\mathbf{u}_{sat} \in \mathbf{R}^{N \times 1}$  expresses the steady-state value of the vector  $\mathbf{u}$ .  $\langle \mathbf{u}_{sat} \rangle$  is a scalar that represents the average of all elements in the vector  $\mathbf{u}_{sat}$ .  $\mathbf{I} \in \mathbf{R}^{N \times 1}$  is a column vector whose elements are all one.

*Proof of Theorem 1:* It is assumed that the system parameters are designed to stabilize the MG. Thus, the resulting voltage vector  $\mathbf{U}$  is a type-1 vector. Based on Lemma 1, all poles of the term  $s(\mathbf{I}_N + \mathbf{L})^{-1}$  lie in the OLHP. It should be noted that if  $\lambda_i$  is an eigenvalue of  $\mathbf{L}$ , then,  $s = -\lambda_i$  is a pole of  $s(\mathbf{I}_N + \mathbf{L})^{-1}$ . The term  $s$  in  $s(\mathbf{I}_N + \mathbf{L})^{-1}$  cancels the pole of  $(\mathbf{I}_N + \mathbf{L})^{-1}$  at the origin. Thus, (33) implies that  $\bar{\mathbf{U}}$  is also a type-1 vector. Since both  $\mathbf{U}$  and  $\bar{\mathbf{U}}$  are type-1, based on the final value theorem

$$\begin{aligned} \lim_{t \rightarrow \infty} \bar{\mathbf{u}}(t) &= \lim_{s \rightarrow 0} s \bar{\mathbf{U}} = \lim_{s \rightarrow 0} s(\mathbf{I}_N + \mathbf{L})^{-1} (s \mathbf{U}) \\ &= \lim_{s \rightarrow 0} s(\mathbf{I}_N + \mathbf{L})^{-1} \times \lim_{s \rightarrow 0} (s \mathbf{U}) \\ &= \mathbf{M} \times \lim_{t \rightarrow \infty} (\mathbf{u}) = \langle \mathbf{u}_{sat} \rangle \mathbf{I} \end{aligned} \quad (36)$$

The active power deviation can be written

$$\delta \mathbf{q} = -b \mathbf{L} \mathbf{q}^{norm} \quad (37)$$

In the steady state, the equations (29) and (30) can be written as

$$\delta \mathbf{u}^1 = \delta \mathbf{u}_0^1 + (\mathbf{G}_P + \mathbf{G}_I(t - t_0))(U_{rate} - \mathbf{M} \mathbf{u}_{sat}) \quad (38)$$

$$\delta \mathbf{u}^2 = \delta \mathbf{u}_0^2 + (\mathbf{H}_P + \mathbf{H}_I(t - t_0))(-b \mathbf{L} \mathbf{q}_{sat}^{norm}) \quad (39)$$

where  $\mathbf{q}_{sat}^{norm}$  expresses the steady-state value of the vector  $\mathbf{q}^{norm} = [\frac{Q_1}{Q_{VRP1}}, \frac{Q_2}{Q_{VRP2}}, \dots, \frac{Q_n}{Q_{VRPn}}]^T$ , thus when system is steady state,

$$\begin{aligned} U_{dref,sat} &= U_{rate} + \delta u^1 + \delta u^2 - n_{opt} Q_{sat} \\ &= U_{rate} + \delta u_0^1 + \delta u_0^2 + \mathbf{G}_P(U_{rate} - \langle \mathbf{u}_{sat} \rangle \mathbf{I}) \\ &\quad + (\mathbf{G}_I(U_{rate} - \langle \mathbf{u}_{sat} \rangle \mathbf{I}) - b \mathbf{H}_I \mathbf{L} \mathbf{q}_{sat}^{norm})(t - t_0) \\ &\quad - b \mathbf{H}_P \mathbf{L} \mathbf{q}_{sat}^{norm} - n_{opt} Q_{sat} \end{aligned} \quad (40)$$

where  $\mathbf{n}_{opt} = \text{diag}\{n_{opti}\}$ ,  $\mathbf{Q}_{sat}$  is the steady-state value of the vector  $\mathbf{Q} = [Q_1, Q_2, \dots, Q_n]^T$ . Equation (40) holds for all  $t \geq t_0$ , and provides a constant voltage set-point vector,  $\mathbf{U}_{dref,sat}$ . Thus, the time-varying part of (40) is zero, expressed as

$$b^{-1} \mathbf{H}_I^{-1} \mathbf{G}_I (\mathbf{U}_{rate} - \langle \mathbf{u}_{sat} \rangle \mathbf{I}) = \mathbf{L} \mathbf{q}_{sat}^{norm} \quad (41)$$

Multiplying both sides of (41) from the left by  $\mathbf{I}^T$

$$\mathbf{I}^T b^{-1} \mathbf{H}_I^{-1} \mathbf{G}_I (\mathbf{U}_{rate} - \langle \mathbf{u}_{sat} \rangle \mathbf{I}) = \mathbf{I}^T \mathbf{L} \mathbf{q}_{sat}^{norm} \quad (42)$$

Given the balanced Laplacian matrix  $\mathbf{I}^T \mathbf{L} = \mathbf{0}$  [27], since  $\mathbf{I}^T b^{-1} \mathbf{H}_I^{-1} \mathbf{G}_I \neq \mathbf{0}$ , there is

$$\mathbf{U}_{rate} = \langle \mathbf{u}_{sat} \rangle \mathbf{I} \quad (43)$$

It can be obtained that,

$$\mathbf{U}_{rate} = \langle \mathbf{u}_{sat} \rangle \quad (44)$$

Therefore, the averaged voltage magnitude,  $\langle \mathbf{u}_{sat} \rangle$  is successfully regulated at the rated value  $U_{rate}$ . By substituting  $\mathbf{U}_{rate} = \langle \mathbf{u}_{sat} \rangle \mathbf{I}$  into (41),

$$\mathbf{L} \mathbf{q}_{sat}^{norm} = \mathbf{0} \quad (45)$$

It is shown in [27] that the only nonzero solution to  $\mathbf{L} \mathbf{x} = \mathbf{0}$  is  $\mathbf{x} = k_q \mathbf{I}$ , where  $k_q$  is any real number. Thus, (23) implies,  $\mathbf{q}_{sat}^{norm} = k_q \mathbf{I}$ , and ensures the reactive power sharing. In the same way, the frequency correction term of (5) is zero in the steady state, there is

$$c \mathbf{L} \mathbf{p}_{sat}^{norm} = \mathbf{0}, \quad \mathbf{p}_{sat}^{norm} = k_p \mathbf{I} \quad (46)$$

where  $\mathbf{p}_{sat}^{norm}$  expresses the steady-state value of the vector  $\mathbf{p}^{norm} = [\frac{P_1}{P_{VRP1}}, \frac{P_2}{P_{VRP2}}, \dots, \frac{P_n}{P_{VRPn}}]^T$ ,  $k_p$  is any real number, this condition satisfies the active power sharing. Finally, combined with (22)-(24), the active and reactive power are all sharing under VRP, there are

$$\begin{aligned} \frac{P_{Magi}}{P_{VRPi}} &= \frac{P_i}{P_{VRPi}} = \frac{1}{\varepsilon_P} = k_p, \\ \frac{Q_{Magi}}{Q_{VRPi}} &= \frac{Q_i}{Q_{VRPi}} = \frac{1}{\varepsilon_Q} = k_q \end{aligned} \quad (47)$$

where  $i = 1, 2, \dots, n$ , so that power can be managed dynamically by adjusting VRP.

#### IV. SIMULATION VALIDATION

In order to verify the effectiveness of the proposed method based on GWO in this paper, we first compare it with other optimization algorithms, PSO, ALO and MFO. The simulation results are shown in Fig. 4.

The results of the objective function (15) are shown in Fig.4(a), and the results of the function F1 in [21] are shown in Fig.4(b). Through the two aspects combined, it is not difficult to find that the convergence speed and optimization results of GWO are better than other optimization algorithms. This is very important for on-line real-time economic scheduling, and why the GWO is chosen.

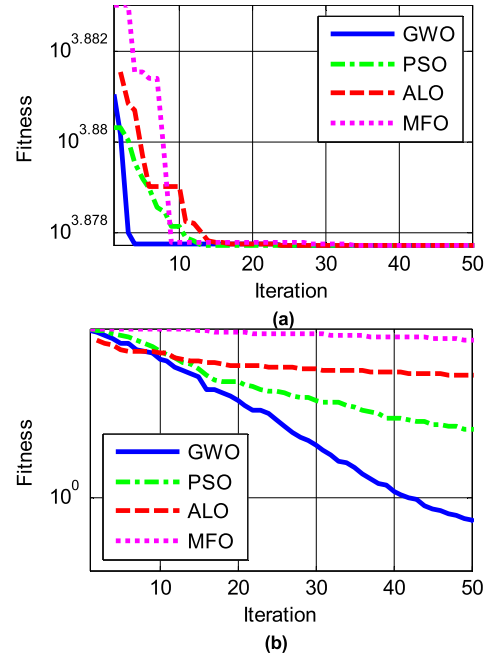


FIGURE 4. Convergence rate contrast graph (a) the objective function (15) (b) the objective function F1 in [21].

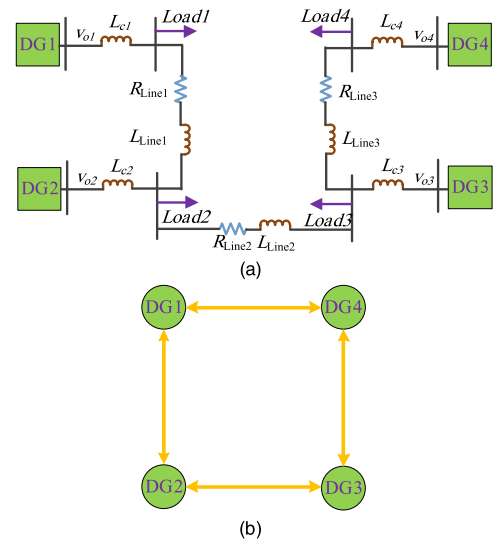
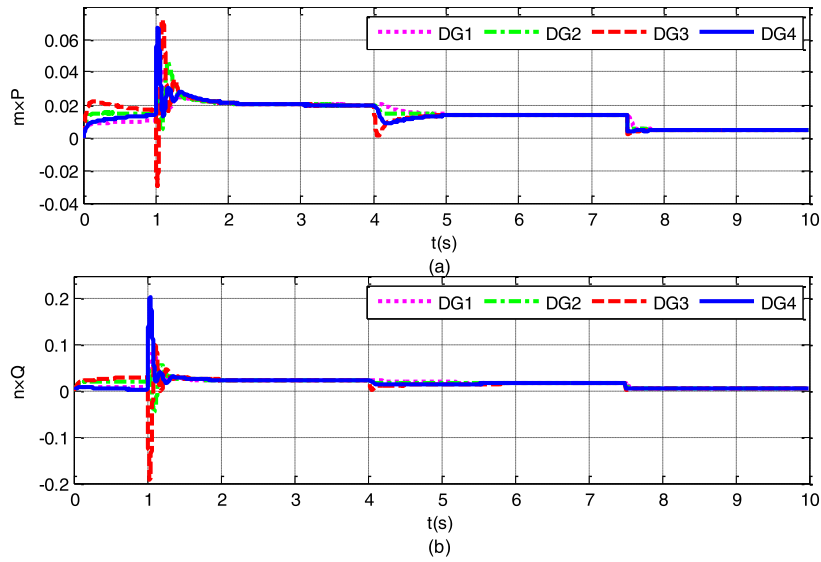


FIGURE 5. System Structure Diagram (a) schematic of the MG physical system (b) communication network.

Next, an experimental system is established to test the performance of the proposed approach as shown in Fig. 5(a). The MG consists of four DGs and the communication topology diagram of the system is shown in Fig. 5(b).

The simulation parameters of each DG are shown in the tables (see Table I and Table II). The voltage reference value is 120V and the angular frequency reference value is 100π (rad/s). The following situations of fixed communication topology and switching topology are considered to verify the effectiveness of the proposed control strategy.



**FIGURE 6.** Performance of the proposed controller with Load3 disconnected (a) DG active power ratios (b) DG reactive power ratios.

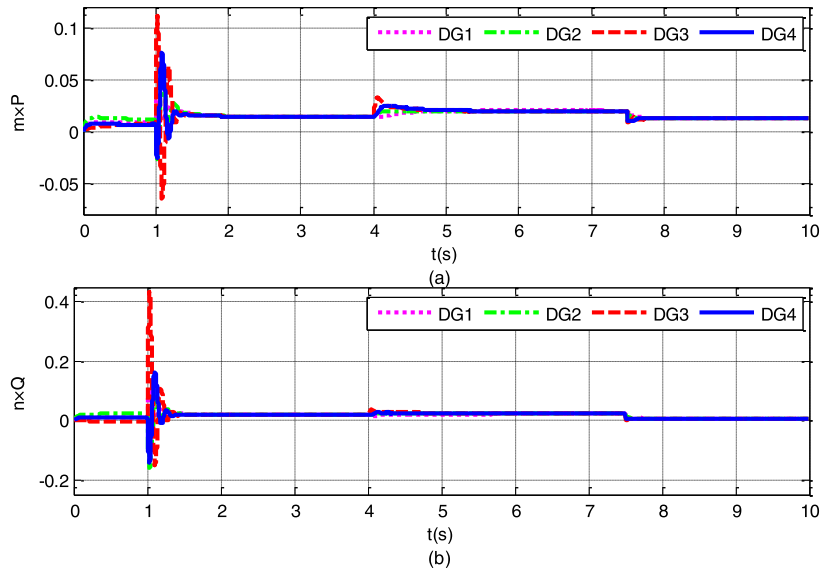


**FIGURE 7.** Performance of the proposed controller with Load3 connected (a) DG active power ratios (b) DG reactive power ratios.

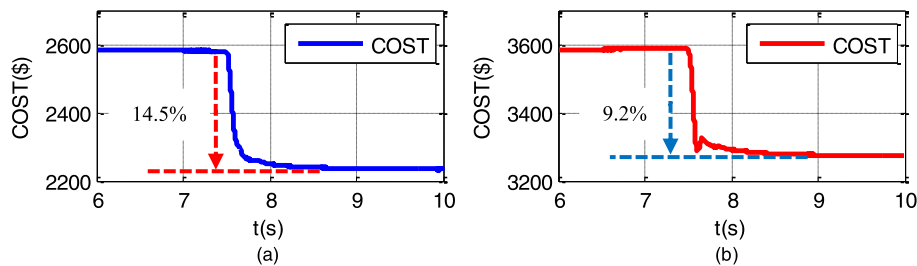


**FIGURE 8.** Cost curve of MG (a) Load3 disconnected (b) Load3 connected.

### A. FIXED COMMUNICATION TOPOLOGY

The MG system operates on islanded mode only with conventional droop control between 0-1s, and the secondary

distributed cooperative control is introduced at 1s. In practical application, connecting and removing of load will affect the active and reactive power sharing of MG. In the case of load



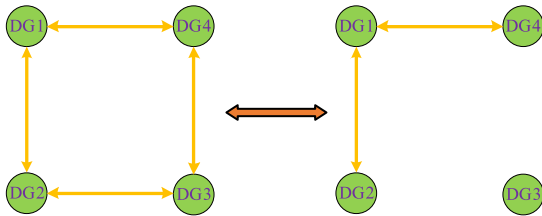


FIGURE 9. Communication network configuration of switching topology.

change, the load 3 is plugged at  $t = 0s$  and removed at  $t = 4s$ , the rest of the system is shown in Fig. 5(a), the simulation results are shown in Fig. 6.

In another case, the load 3 is removed at  $t = 0s$  and plugged at  $t = 4s$ , the simulation results are shown in Fig. 7. In order to verify the effectiveness of GWO algorithm, this paper introduces GWO at  $t = 7.5s$ . The cost curves for the above two cases are shown in Fig. 8(a) and Fig. 8(b), respectively.

From Fig. 6 and Fig. 7, we can see that the power sharing is not achieved with conventional droop control before  $t = 1s$ . Under the influence of secondary control,  $m_{opti}P_{Magi}$  and  $n_{opti}Q_{Magi}$  are all equal to each other, respectively. It means that the active and reactive power are all sharing under VRP.

Based on the (16), the cost curve of the system is shown in Fig. 8(a) and Fig. 8(b), corresponding to Fig. 6 and Fig. 7,

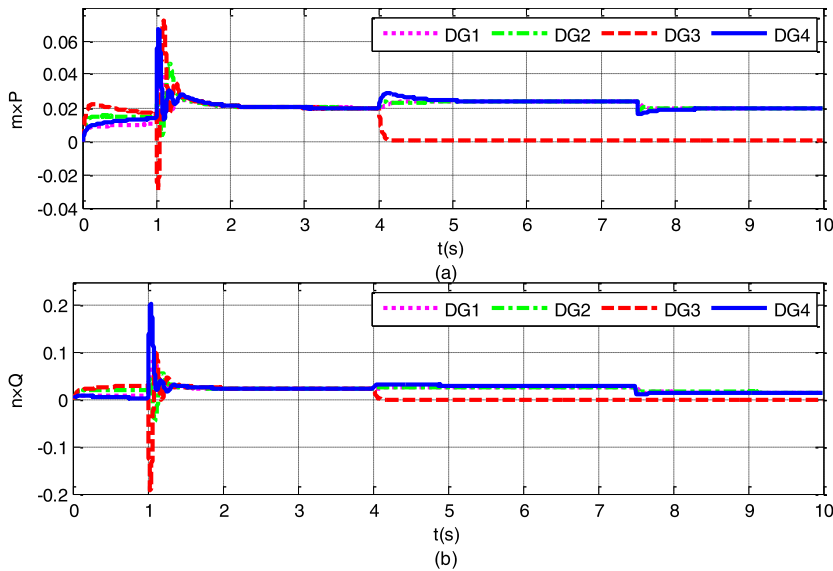


FIGURE 10. Performance of the proposed controller with DG3 disconnected (a) DG active power ratios (b) DG reactive power ratios.

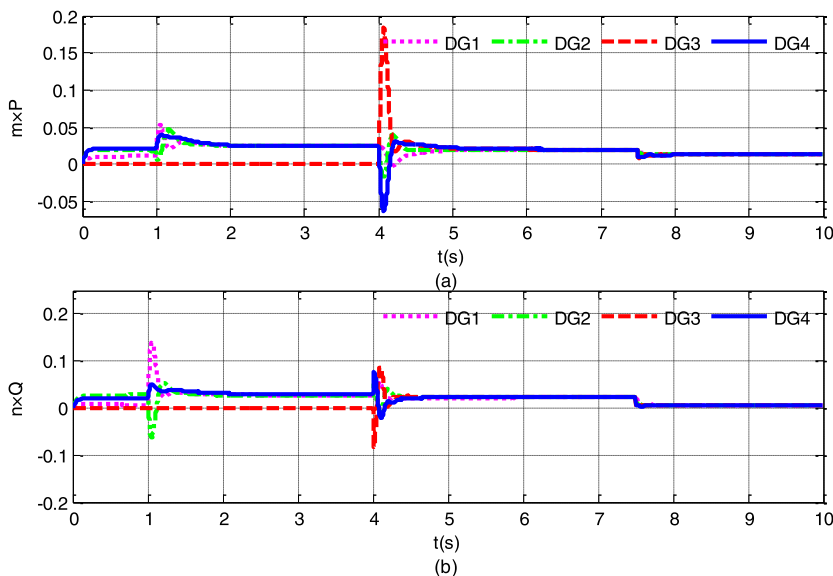


FIGURE 11. Performance of the proposed controller with DG3 connected (a) DG active power ratios (b) DG reactive power ratios.

respectively. It can be seen that the cost of the first case decreases by 14.5% and the one of the second case decreases by 9.2% under GWO. The effectiveness of the proposed algorithm is obvious.

**B. SWITCHING COMMUNICATION TOPOLOGY**

It is assumed that DGs communicate with each other through the communication digraph depicted in Fig. 9. The first case, the communication links between DG2 and DG3 are connected at  $t = 0s$  and disconnected at  $t = 4s$ , while the communication links between DG3 and DG4 are the same.

The simulation results are shown in Fig. 10. In another case, the DG3 is removed at  $t = 0s$  and plugged at  $t = 4s$ , the simulation results are shown in Fig. 11. Similar to the previous section, GWO was introduced at  $t = 7.5s$ . The cost curves for the above two cases are shown in Fig. 12(a) and Fig. 12(b), respectively.

As shown in Fig. 10 and Fig. 11, when DG3 is separated from the system, the system can still achieve power sharing. In this way, the plug-and-play is realized. Based on the (16), the cost curve of the system is shown in Fig. 12(a) and Fig. 12(b), corresponding to Fig. 10 and Fig. 11, respectively.

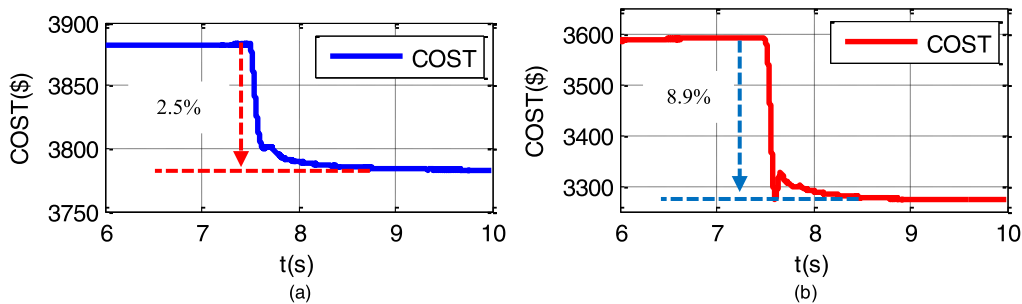


FIGURE 12. Cost curve of MG (a) DG3 disconnected (b) DG3 connected.

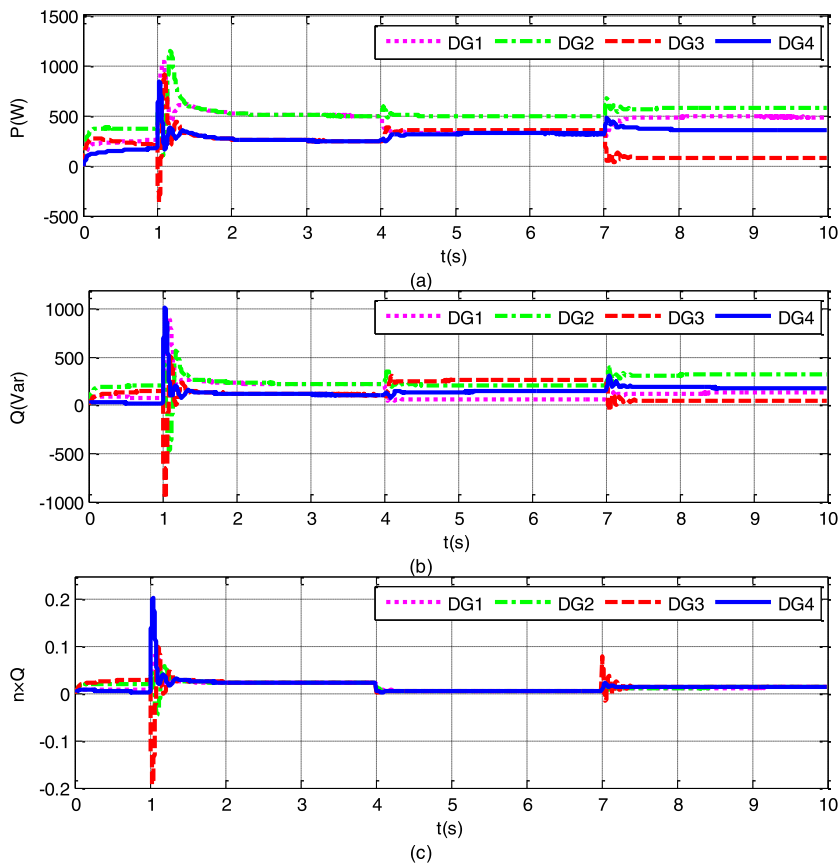


FIGURE 13. Performance of the controller with variable cost coefficient (a) DG active power (b) DG reactive power (c) DG reactive power ratios.

It can be seen that the cost of the first case decreases by 2.5% and the one of the second case decreases by 8.9% under GWO. When DG3 is disconnected, the system has three agents left, which makes the adjustable space relatively smaller. When DG3 is restored, the system has four agents, which makes the adjustable space relatively larger. That's why the cost reduction in the first case is less than that in the second case.

**C. VARIABLE COST COEFFICIENT**

If the cost coefficient changes abruptly in the operation of the system, the method proposed in this paper can realize the automatic management of energy. In this case, GWO is started at  $t = 4s$ . The cost coefficient  $A_3$  in (16) changes from 1\$/W to 3\$/W at  $t = 7s$ . The simulation results are shown in Fig. 13.

It can be seen from Fig. 13(a) and Fig. 13(b), when the cost coefficient of DG3 increases, the system automatically reduces the power output of DG3 to save cost. Meanwhile the power sharing can still be achieved, as shown in Fig. 13(c). These good performances show that the method proposed in this paper is effective.

**V. CONCLUSION**

The optimal power allocation scheme of MG is proposed in this paper by considering economic factors based on the theory of multi-agent consistency and GWO at the secondary control level.

- 1) The secondary controller is constructed based on multi-agent consensus theory, which makes the control of MG more flexible and reliable. In this way, we obtain the active and reactive power sharing. The load and DG can be switched freely during the operation of the system, i.e., the plug-and-play capability of the system is realized.
- 2) The concept of virtual rated power (VRP) is proposed. Combining the calculation results of GWO and secondary controller, the optimal power allocation scheme is obtained, considering the economic dispatching problem. Moreover, the more DG, the greater the cost reduction.
- 3) The real-time on-line cost coefficient adjustment is realized by utilizing the nature of multi-agent consensus theory, i.e., when the power generation cost of one DG changes, the power allocation scheme could automatically allocates energy to achieve the cost reduction.

The validation of the proposed algorithm can be achieved by connecting MATLAB with the experimental equipment through special instruments. Due to the limitation of conditions, the author has not been able to verify the effectiveness of the proposed method through experiments. Experimental verification and practical application will be the focus of author's future research.

**APPENDIX**

**TABLE 1. Simulation parameters of each DG.**

Symbol	Quantity	DG1&DG2	DG3&DG4
$U_{dc}$	Dc-bus voltage	300 V	300 V
$\omega_{rate}$	Rated angular velocity	100 rad/s	100 rad/s
$P_{ratei}$	Rated active power	800 W	400W
$Q_{ratei}$	Rated reactive power	600 Var	300 Var
$U_{rate}$	Rated voltage	120V	120V
$n_i$	Reactive droop coefficient	0.01 V/Var	0.02 V/Var
$m_i$	Active droop coefficient	$4 \times 10^{-4}$ rad/(s*W)	$8 \times 10^{-4}$ rad/(s*W)
$Q$	Reactive power load	100&200 Var	100&50 Var
$P$	Active power load	200&400 W	300&100 W
$L_f$	Filter inductance	1.8 mH	1.8mH
$R$	Filter resistance	0.1 $\Omega$	0.1 $\Omega$
$C_f$	Filter capacitor	50 $\mu$ F	50 $\mu$ F
$\omega_c$	Cut-off frequency of the filter	25 rad/s	25 rad/s
$L_c$	Output end inductance	1.4&0.35 mH	0.7&1.05 mH
$A_i$	Cost coefficient	2&1.7 \$/W	1&1.5 \$/W
$b$	Designed parameter	30	30
$c$	Designed parameter	0.1	0.1
$k_{pQ}$	$G_i(s)$ proportional term	0.01	0.01
$k_{iQ}$	$G_i(s)$ integral term	3	3
$k_{pv}$	$H_i(s)$ proportional term	0.005	0.005
$k_{iv}$	$H_i(s)$ integral term	2	2

Note: the designed parameter  $A_G$  as follows:

$$A_G = 1.6 \times \begin{bmatrix} 0 & 1 & 0 & 1 \\ 1 & 0 & 1 & 0 \\ 0 & 1 & 0 & 1 \\ 1 & 0 & 1 & 0 \end{bmatrix}$$

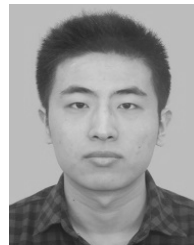
**TABLE 2. Simulation parameters of system.**

Symbol	Quantity	Value
$\eta$	Weight coefficient	2
$\lambda$	Weight coefficient	1
$i_{j\_Max}$	Iteration times of GWO	500
$num$	Number of wolves	200
$L_{Line1}$	Line inductance	5.0 mH
$R_{Line1}$	Line resistance	0.2 $\Omega$
$L_{Line2}$	Line inductance	1.5 mH
$R_{Line2}$	Line resistance	0.3 $\Omega$
$L_{Line3}$	Line inductance	2.0 mH
$R_{Line3}$	Line resistance	0.4 $\Omega$

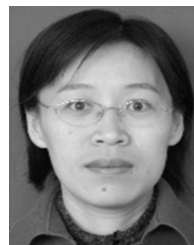
**REFERENCES**

[1] H. M. Goodarzi and M. H. Kazemi, "An optimal autonomous microgrid cluster based on distributed generation droop parameter optimization and renewable energy sources using an improved grey wolf optimizer," *Eng. Optim.*, vol. 50, no. 5, pp. 819–839, Aug. 2017.

- [2] C. Chen, S. Duan, B. Liu, and G. Hu, "Smart energy management system for optimal microgrid economic operation," *IET Renew. Power Generat.*, vol. 5, no. 3, pp. 258–267, 2011.
- [3] O. Hafez and K. Bhattacharya, "Optimal planning and design of a renewable energy based supply system for microgrids," *Renew. Energy*, vol. 45, pp. 7–15, Sep. 2012.
- [4] D. Apostolopoulou, P. Sauer, and A. Domínguez-García, "Automatic generation control and its implementation in real time," in *Proc. Hawaii Int. Conf. Syst. Sci. (HICSS)*, Waikoloa, HI, USA, Jan. 2014, pp. 2444–2452.
- [5] L. Na, L. Chen, C. Zhao, and S. H. Low, "Connecting automatic generation control and economic dispatch from an optimization view," in *Proc. Amer. Control Conf.*, Portland, OR, USA, Jun. 2014, pp. 735–740.
- [6] Y. A. Abass, A. T. Al-Awami, and T. Jamal, "Integrating automatic generation control and economic dispatch for microgrid real-time optimization," in *Proc. IEEE Power Energy Soc. General Meeting (PESGM)*, Jul. 2016, pp. 1–5.
- [7] J. J. Liu, Z. J. Wang, Y. Z. Ye, and Z. H. Zhang, "Research for PV cell and storage battery of dynamic economic dispatch in micro-grid," *Adv. Mater. Res.*, vols. 998–999, pp. 458–461, Jul. 2014.
- [8] S. Sharma, S. Bhattacharjee, and A. Bhattacharya, "Grey wolf optimization for optimal sizing of battery energy storage device to minimise operation cost of microgrid," *IET Gener., Transmiss. Distrib.*, vol. 10, no. 3, pp. 625–637, 2016.
- [9] A. A. Moghaddam, A. Seifi, T. Niknam, and M. R. A. Pahlavani, "Multi-objective operation management of a renewable MG (micro-grid) with back-up micro-turbine/fuel cell/battery hybrid power source," *Energy*, vol. 36, no. 11, pp. 6490–6507, Nov. 2011.
- [10] S. Mashayekh, M. Stadler, G. Cardoso, and M. Heleno, "A mixed integer linear programming approach for optimal DER portfolio, sizing, and placement in multi-energy microgrids," *Appl. Energy*, vol. 187, pp. 154–168, Feb. 2017.
- [11] Y. Du, W. Pe, N. Chen, X. Ge, and H. Xiao, "Real-time microgrid economic dispatch based on model predictive control strategy," *J. Modern Power Syst. Clean Energy*, vol. 5, no. 5, pp. 787–796, Sep. 2017.
- [12] W. Liu, W. Gu, W. Sheng, X. Meng, Z. Wu, and W. Chen, "Decentralized multi-agent system-based cooperative frequency control for autonomous microgrids with communication constraints," *IEEE Trans. Sustain. Energy*, vol. 5, no. 2, pp. 446–456, Apr. 2014.
- [13] C. Huang, S. Weng, D. Yue, S. Deng, J. Xie, and H. Ge, "Distributed cooperative control of energy storage units in microgrid based on multi-agent consensus method," *Electr. Power Syst. Res.*, vol. 147, pp. 213–223, Jun. 2017.
- [14] X. Wang, H. Zhang, and C. Li, "Distributed finite-time cooperative control of droop-controlled microgrids under switching topology," *IET Renew. Power Gener.*, vol. 11, no. 5, pp. 707–714, Apr. 2017.
- [15] F. Guo, C. Wen, J. Mao, and Y. D. Song, "Distributed secondary voltage and frequency restoration control of droop-controlled inverter-based microgrids," *IEEE Trans. Ind. Electron.*, vol. 62, no. 7, pp. 4355–4364, Jul. 2015.
- [16] N. M. Dehkordi, N. Sadati, and M. Hamzeh, "Fully distributed cooperative secondary frequency and voltage control of islanded microgrids," *IEEE Trans. Energy Convers.*, vol. 32, no. 2, pp. 675–685, Jun. 2017.
- [17] A. Askarzadeh, "A memory-based genetic algorithm for optimization of power generation in a microgrid," *IEEE Trans. Sustain. Energy*, vol. 9, no. 3, pp. 1081–1089, Jul. 2018.
- [18] B. Zhao, X. Zhang, P. Li, K. Wang, M. Xue, and C. Wang, "Optimal sizing, operating strategy and operational experience of a stand-alone microgrid on Dongfushan Island," *Appl. Energy*, vol. 113, no. 2, pp. 1656–1666, Jan. 2014.
- [19] B. Bahmani-Firouzi and R. Azizpanah-Abarghoee, "Optimal sizing of battery energy storage for micro-grid operation management using a new improved bat algorithm," *Int. J. Elect. Power Energy Syst.*, vol. 56, pp. 42–54, Mar. 2014.
- [20] A. A. Moghaddam, A. Seifi, and T. Niknam, "Multi-operation management of a typical micro-grids using particle swarm optimization: A comparative study," *Renew. Sustain. Energy Rev.*, vol. 16, no. 2, pp. 1268–1281, 2012.
- [21] S. Mirjalili, S. M. Mirjalili, and A. Lewis, "Grey wolf optimizer," *Adv. Eng. Softw.*, vol. 69, pp. 46–61, Mar. 2014.
- [22] M. Akbari, M. A. Golkar, and S. M. M. Tafreshi, "Firefly algorithm-based voltage and frequency control of a hybrid AC-DC microgrid," in *Proc. 17th Conf. Elect. Power Distrib.*, May 2012, pp. 1–7.
- [23] S. Mirjalili, "Moth-flame optimization algorithm: A novel nature-inspired heuristic paradigm," *Knowl.-Based Syst.*, vol. 89, pp. 228–249, Nov. 2015.
- [24] K. Nimma, M. Al-Falahi, H. D. Nguyen, S. D. G. Jayasinghe, and M. Negnevitsky, "Grey wolf optimization-based optimum energy-management and battery-sizing method for grid-connected microgrids," *Energies*, vol. 11, no. 4, p. 847, Apr. 2018.
- [25] A. Bidram, A. Davoudi, F. L. Lewis, and J. M. Guerrero, "Distributed cooperative secondary control of microgrids using feedback linearization," *IEEE Trans. Power Syst.*, vol. 28, no. 3, pp. 3462–3470, Aug. 2013.
- [26] R. Olfati-Saber and R. M. Murray, "Consensus problems in networks of agents with switching topology and time-delays," *IEEE Trans. Autom. Control*, vol. 49, no. 9, pp. 1520–1533, Sep. 2004.
- [27] V. Nasirian, S. Moayedi, A. Davoudi, and F. L. Lewis, "Distributed cooperative control of dc microgrids," *IEEE Trans. Power Electron.*, vol. 30, no. 4, pp. 2288–2303, Apr. 2015.



**JIANCHENG ZHANG** received the B.S. degree from Hebei Polytechnic University, Tangshan, China, in 2010, the M.S. degree from the Harbin Institute of Technology, Shenzhen, China, in 2013. He is currently pursuing the Ph.D. degree in Harbin Institute of Technology, Harbin, China. His research interests include multi-agent cooperative control and grid-connected algorithm for microgrid.



**XINSHENG WANG** received the B.S., M.S., and Ph.D. degrees from the Harbin Institute of Technology, Harbin, China, in 1992, 1995, and 2002, respectively. She is currently an Associate Professor of control science and engineering with the Harbin Institute of Technology, Weihai, China. Her research interests include robust and nonlinear control and power electronics system modeling and control.



**LINGYU MA** received the B.S. degree from Shandong Jianzhu University, Jinan, China, in 2011, and the M.S. degree from the Harbin Institute of Technology, Shenzhen, China, in 2013. She is currently a Lecturer of control science and engineering with Shandong Management University, Jinan. Her research interests include robust and nonlinear control, development, and the application of embedded systems.

...